Anal. Calcd for $C_4H_2OS_4$ (**22**): C, 24.72; H, 1.04; S, 66.00. Found: C, 24.70; H, 1.12; S, 66.07.

Preparation of Dimethyl Tetrathiooxalate (18) by Gas-Phase Pyrolysis. 4,5-Bis(methylthio)-1,3-dithiol-2-one (0.3 g, 1.4 mmol) was sublimed (150 °C) into a hot quartz tube (25 × 1.6 cm, 450 °C) and the pyrolysate collected in a liquid N_2 trap (pressure behind the trap ca. 5×10^{-3} torr). The pyrolysate was dissolved in acetone, filtered, and purified by column chromatography (2.5 × 10 cm, silica gel, 0.063–0.200 mm thick, CCl_4). The dark solution was concentrated and cooled to yield 0.14 g (54%) of pure **18**, mp 66 °C; MS *m/e* 182 (M^+); IR (KBr) $\tilde{\nu}_{max}$ 2990 cm^{-1}, 2910, 1410, 1395, 1310, 1080, 1050, 945, 770, 700; ^1H NMR ($CDCl_3$) δ 2.64.

Lit.[19]: mp 66 °C; IR (KBr) $\tilde{\nu}_{max}$ 2980 cm^{-1}, 2900, 1415, 1400, 1310, 1045, 945, 770, 700.

Note Added in Proof. Professor Heilbrohher has kindly provided us with a preprint of a paper[46] reporting the He I photoelectron spectra of some stable 1,2-olithietes, including the recently synthesized 3,4-di-*tert*-butyl-1,2-dithiete.[47]

Acknowledgment. This work was supported by the Deutsche Forschungsgemeinschaft and the Fonds der Chemischen Industrie. The calculations were carried out on the TR 440 computer at the University of Marburg. We thank Dr. G. Schaden for performing preparative pyrolysis experiments.

Registry No. **1**, 360-91-8; **8**, 2314-40-1; **9**, 49675-88-9; **10**, 934-31-6; **11**, 7092-01-5; **12**, 23783-27-9; **14**, 74378-81-7; **18**, 61485-47-0; **19**, 61485-46-9; **20**, 85720-61-2; **21**, 77102-71-7; **22**, 85720-62-3; **23**, 74962-29-1; **24**, 74962-30-4; **25**, 85720-63-4; **26**, 85720-64-5; 4,5-dimethyl-1,3-dithiol-2-thione, 17534-27-9; 4,5-bis(ethylthio)-1,3-dithiol-2-thione, 59065-21-3; 4,5-bis(isopropylthio)-1,3-dithiol-2-thione, 77102-72-8; 2,4,6,8-tetrathiabicyclo[3.3.0]oct-1(5)-ene-7-thione, 70800-59-8.

(46) Fiah-gi, W.; Mahraz, M.; Heilbrohher, E.; Krebs, A.; Schütz, K.; Voss, J.; Köpke, B. *Helv. Chim. Acta*, in press.

(47) Köpke, B.; Voss, J. *J. Chem. Res., Synop.* **1982**, 314.

Variable Pressure and Temperature Nuclear Magnetic Resonance and Visible Spectrophotometric Studies of Lanthanide Ions in Dimethylformamide: Solvation and Solvent Exchange Dynamics[1]

Dino L. Pisaniello, Lothar Helm, Pierre Meier, and André E. Merbach*

Contribution from the Institut de chimie minérale et analytique, University of Lausanne, 3, Place du Château, 1005 Lausanne, Switzerland. *Received December 13, 1982*

Abstract: The equilibrium $[Ln(DMF)_8]^{3+} + DMF \rightleftharpoons [Ln(DMF)_9]^{3+}$ has been studied in solutions of lanthanide perchlorates. For Nd the following thermodynamic parameters were obtained from spectrophotometric studies: $\Delta H = -14.9 \pm 1.3$ kJ mol^{-1}, $\Delta S = -69.1 \pm 4.2$ J K^{-1} mol^{-1} and $\Delta V = -9.8 \pm 1.1$ cm^3 mol^{-1}. The NMR study of Ln = Ce–Nd and Tb–Yb shows that the coordination equilibria also take place for the other light lanthanides. At room temperature the major species is $[Ln(DMF)_8]^{3+}$ when Ln = Ce–Nd, and this becomes the only stable species when Ln = Tb–Lu. Characteristic ^{17}O, ^{13}C, and ^1H NMR shifts for $[Ln(DMF)_8]^{3+}$ are also reported. Kinetic parameters for the exchange of DMF on $[Ln(DMF)_8]^{3+}$ (Ln = Ty–Yb) have been determined by variable temperature and pressure ^1H NMR in neat DMF. For Tb, ΔH^* (kJ mol^{-1}), ΔS^* (J mol^{-1} K^{-1}) and ΔV^* (cm^3 mol^{-1}) are respectively 14.1 ± 0.4, −58 ± 2, and +5.2 ± 0.2 while for Yb the corresponding values are 39.3 ± 0.6, +40 ± 3, and +11.8 ± 0.4. The observed systematic variations in activation parameters from Tb to Yb are interpreted in terms of a mechanistic crossover at Er. Kinetic rate law determinations in CD_3NO_2 diluent indicate than an interchange mechanism operates for Tb (K_{os} = 0.5 mol^{-1} kg at 231 K) whereas a D mechanism is operative for Yb.

Introduction

The tripositive lanthanides constitute the longest series of chemically similar metal ions and exhibit a steady decrease in ionic radius of from lanthanum to lutecium. In view of the insignificance of effects attributable to ligand fields (e.g., preference for certain coordination polyhedra) or ligand π orbital back-bonding, a study of these ions in solution provides an opportunity to closely assess any observed variations in solvation and solvent exchange kinetics in simple electrostatic and steric terms.

While considerable effort has gone into attempts at understanding lanthanide hydration and the kinetics of water exchange, it appears that the inherently great labilities of these ions are largely responsible for the paucity of accurate data. Indeed, Marcus[3] has recently discussed lanthanide aquo ions from various standpoints and has highlighted a large number of uncertainties. For example, controversy[4,5] still exists as to whether there is a change in coordination number (nine to eight) across the series. From a kinetic viewpoint, extension of the research dealing with aqueous solutions to include nonaqueous solvents has been informative and has yielded accurate DMF (*N,N*-dimethylformamide) exchange parameters for $[Tm(DMF)_8]^{3+}$ by ^{13}C and ^1H NMR.[6] The present work seeks to establish the kinetics and mechanisms of DMF exchange for other members of the lanthanide series by variable temperature and pressure studies.

Experimental Section

A. Materials and Preparation of Solutions. Lanthanide oxides (Research Chemicals, 99.9%) and hydrated cerium(III) perchlorate (Ventron) were used as received. DMF (Fluka, puriss) was purified by fractional distillation at reduced pressure. Benzene (Merck, p.a.), dichloromethane, and nitromethane (Fluka, puriss) were redistilled before

(1) This paper is to be considered part 19 of the series, "High Pressure NMR Kinetics". For part 18, see ref 2.

(2) Tregloan, P. A.; Helm, L.; Meier, P.; and Merbach, A. E. *Inorg. Chim. Acta*, in press.

(3) Marcus, Y. *Gmelin Handbuch* **1981**, *D3*, 1.

(4) Spedding, F. H.; Pikal, M. J.; Ayers, B. O. *J. Phys. Chem.* **1966**, *70*, 2440.

(5) (a) Reuben, J.; Fiat, D. *J. Chem. Phys.* **1969**, *51*, 4909. (b) Grenthe, I.; Hessler, G.; Hots, H. *Acta Chem. Scand.* **1973**, *65*, 573.

(6) Pisaniello, D. L.; Merbach, A. E. *Helv. Chim. Acta* **1982**, *65*, 573.

0002-7863/83/1505-4528$01.50/0

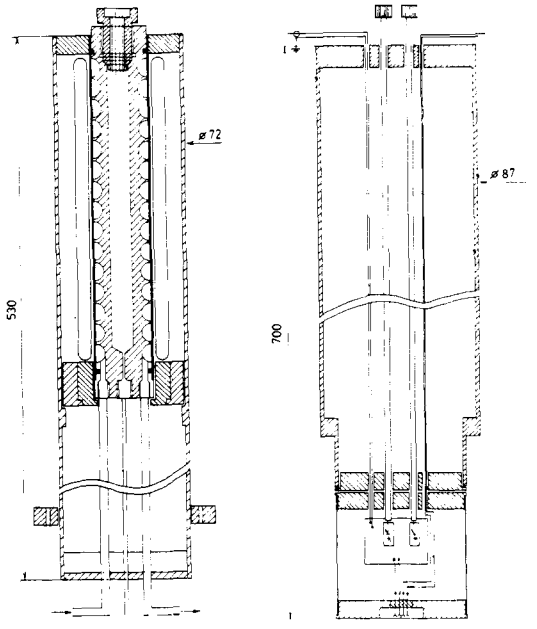

Figure 1. Schematic drawing of the wide-bore superconducting magnet multinuclear high-pressure probe (///, aluminum of Berylco; \\\, Teflon or Vespel): (left) lower aluminum support and high pressure bomb (above); (right) upper aluminum support and capacitive adapter box (below).

use. Deuterated nitromethane (Ciba-Geigy) was used as received. All liquid reagents were stored in dark bottles over previously activated 4Å molecular sieves. $[Ln(DMF)_8](ClO_4)_3$ complexes, Ln = La–Nd and Tb–Lu, were prepared as previously described,[6] with the yields of the hygroscopic compounds being essentially quantitative. The metal content was determined by EDTA titration[7] and/or by an ion-exchange technique[8] and gave the following apparent solid state coordination numbers: La, 8.2; Ce, 7.9; Pr, 7.9; Nd, 8.0; Tb, 7.9; Dy, 8.2 Ho, 7.8; Er, 8.0; Tm, 8.0; Yb, 8.0; Lu, 8.0. Solutions for NMR study were prepared by weight in a glove box (water < 6 ppm). The internal ^1H NMR chemical shift reference was 1% w/w benzene. Spectrophotometric solutions were made up in 10 cm^3 volumetric flasks in the glove box.

B. Spectrophotometric Measurements. Visible spectra were recorded on a Perkin-Elmer Hitachi 340 spectrophotometer with a 0.15-nm bandpass. Variable temperature experiments were carried out with 5-cm path length thermostated cells in double beam mode. A 100-Ω Pt resistance, in contact with the thermostating fluid near the cell jacket inlets, was used to measure the temperature. No significant temperature gradient was detected across the solution inside the cell.

For high-pressure experiments, a le Noble–Schlott[9] optical cell was employed. A 100-Ω Pt resistance, in contact with methylcyclohexane, the pressure transmission fluid, was used to monitor the temperature, the stability of which was better than ±0.2 K over several hours.

C. NMR Measurements. Variable temperature Fourier transform ^1H NMR spectra were obtained with Bruker WH-360, CXP-200, and WP-60 instruments operating at 360, 200, and 60 MHz, respectively, with an internal deuterium lock. For measurements in neat solvent, precision bore coaxial NMR tubes (Wilmad) were employed. The 2 mm o.d. inner tube contained the sample, while the outer tube incorporated the lock substance (CD_2Cl_2 or $C_2D_2Cl_4$). For measurements in the diluent CD_3NO_2, 5-mm o.d. tubes were used and the deuterium signal was used as a lock. T_2 measurements were made from the full width at half height of the NMR absorption resonance. ^1H chemical shifts were measured relative to the internal reference but ultimately reported relative to pure DMF. The temperature dependence of the pure DMF line widths and the internal reference DMF shifts were determined from the appropriate "blank" samples and taken into account for subsequent calculations. Natural abundance ^{17}O and ^1H-decoupled ^{13}C spectra were run at 27.1 and 50.3 MHz, respectively, on the CXP-200 spectrometer without lock; 9-mm spheres were used to eliminate susceptibility differences between samples. Sample temperatures were measured before and after spectral accumulation by substituting the sample with a calibrated

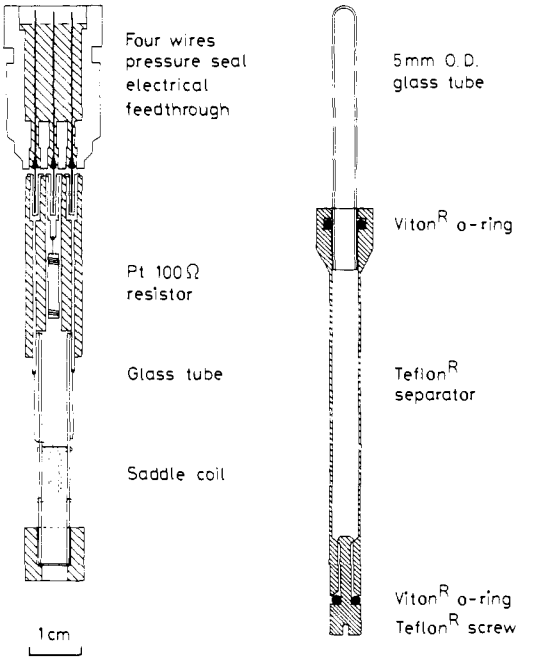

Figure 2. Pressure seal and internal components of the bomb (left); sample tube and separator assembly (right).

platinum resistance[10] immersed in a solution of identical composition or by substitution with methanol or ethylene glycol samples.

Variable pressure ^1H spectra were run on the CXP-200 and WP-60 instruments. The high-pressure probe head used for the WP-60 was a slightly modified version of one previously described.[11] An external ^{19}F lock was incorporated.

For the high-pressure experiments on the CXP-200 spectrometer, a multinuclear probe was built. It fits into the tubular wide-bore (ϕ 89 mm) of the 4.7 Tesla Bruker B-C 47/90 superconducting magnet. The probe, made of four separable parts, is shown schematically in Figure 1. The lower aluminum support is introduced into the magnet from the bottom and fixed by a flange adjustable in height. This allows the pressure bomb to be positioned in the region of highest field homogeneity. The pressure bomb is made of a nonmagnetic beryllium–copper alloy, Berylco-25, and has been tested up to 250 MPa. It has an external diameter of 31 mm. A double helix is cut in the outside of the bomb, for circulation of the thermostating liquid, so that the external diameter for supporting pressure is actually 21 mm, with an internal diameter of 12 mm. The double helix is covered with a thin cylindrical Berylco jacket. For thermal insulation with the magnet the bomb is surrounded by a glass Dewar. The inside top of the bomb is provided with a conical surface and threads for a modified Bridgeman seal. At the bottom there are three threaded connections, one for the pressurizing liquid, the two others for the inlet and outlet of the thermostating liquid.

The upper aluminum support and the frequency adapter box are inserted into the tuning magnet from the top. The adapter box contains a capacitive tuning network which is specific for a small frequency range. This box must therefore be changed when changing the observed nuclei. Three boxes have been built: for ^1H (200 MHz), ^{13}C (50.3 MHz), and ^{17}O (27.1 MHz). The corresponding capacitive tuning networks have been designed according to Hoult.[12] The adapter boxes are connected to the pressure seal of the bomb by a four-pin plug. The upper aluminum support contains two screwdrivers for access to the trimmer capacitors in the tuning network; it supports the radiofrequency plug for connection with the spectrometer transmitter and receiver, and it also supports the plug for connecting the platinum resistance to an ohmmeter for temperature measurements.[13]

The internal components of the bomb and the sample tube are shown in Figure 2. The saddle-shaped coil (the same for the three nuclei) is made of two 0.2-mm copper wires and has a diameter of 7 mm and a

(7) Brunisholz, G.; Quinche, J. P.; Kalo, A. M. *Helv. Chim. Acta* **1964**, *47*, 14.
(8) Vogel, A. I. "Quantitative Inorganic Analysis", 3rd ed.; Longmans Green and Co.: London, 1961; p 702.
(9) le Noble, W. J.; Schlott, R. *Rev. Sci. Instrum.* **1976**, *47*, 770.
(10) Ammann, C.; Meier, P.; Merbach, A. E. *J. Magn. Reson.* **1982**, *46*, 319.
(11) (a) Vanni, H.; Earl, W. L.; Merbach, A. E. *J. Magn. Reson.* **1978**, *29*, 11. (b) Earl, W. L.; Vanni, H.; Merbach, A. E. *Ibid.* **1978**, *30*, 571. (c) Monnerat, A.; Moore, P.; Newman, K. E.; Merbach, A. E. *Inorg. Chim. Acta* **1981**, *47*, 139.
(12) Hoult, D. I. *Prog Nucl. Magn. Reson. Spectrosc.* **1978**, *12*, 41.
(13) Meyer, F. K.; Merbach, A. E. *J. Phys. E: Sci. Instrum.* **1979**, *12*, 185.

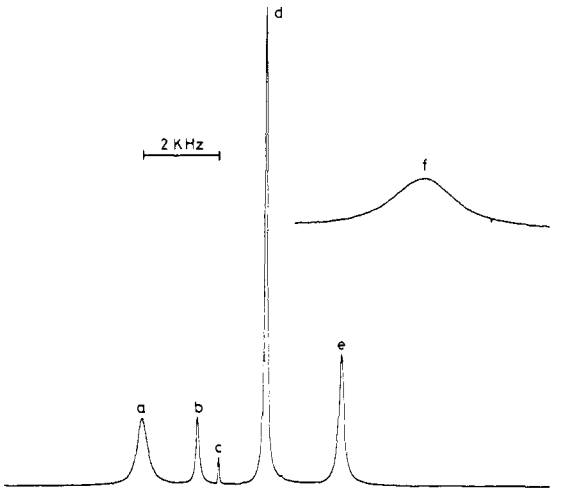

Figure 3. 360 MHz ^1H NMR spectrum of a $[Yb(DMF)_8](ClO_4)_3$/DMF/CD_2Cl_2 solution (P_m = 0.501) at 175 K. The resonances a–f (increasing field) are assigned as follows: (a) N–CH_3 trans to formyl proton of coordinated DMF; (b) formyl proton of free DMF; (c) residual proton impurity of incompletely deuterated CD_2Cl_2; (d) both N–CH_3 resonances of free DMF; (e) N–CH_3 cis to formyl proton of coordinated DMF; (f) formyl proton of coordinated DMF. Resonance f (displayed at higher amplitude) is 20.8 kHz upfield of c.

height of 10 mm. It is wound on a thin-walled borosilicate glass tube with an internal diameter of 5.5 mm. A commercial platinum resistor (Heraeus, Pt 100 Ω GS 1218) is placed just above the sample tube for temperature measurements; the temperature is obtained with a standard, DIN 43760, $T = f(\Omega)$ conversion table and taking into account the slight effect of pressure on the resistance.[13] The passage through the bomb of the radiofrequency and Pt resistor wires is made with a four-wire pressure seal electrical feedthrough similar to that described elsewhere.[13] No coaxial transmission line, as proposed by Jonas[14] for high-pressure ^1H NMR at 180 MHz, was found necessary. The glass sample tube is a commercial 5 mm o.d. tube (Wilmad Co.) cut to the right length. The separator, made of Teflon, transmits the hydrostatic pressure to the sample. Two Viton O-rings are used: for connection to the sample tube and to ensure tightness of the closing Teflon screw. The sample tube and separator assembly requires 2.5 mL of sample solution. The surrounding pressure transmitting liquids used are 1,2-dibromo-1,1,2,2-tetrafluoroethane (Fluobrene) for low temperatures (<300 K), and 1,1,2,2-tetrachloroethene for higher temperatures. These liquids were chosen because they do not contain protons, the most frequently observed nuclei; in special cases other liquids may be used. The pressure is generated with a standard system consisting of a pneumatic pump, a separator and valves (Nova Swiss Co.), and a Heise Bourdon gauge. The temperature is regulated by circulating ethanol (–60 to +30 °C) or oil (+30 to 150 °C) around the bomb by use of a high capacity cryo- or thermostat. The temperature range, at the present time, is essentially limited by the available thermostating units. The spectral resolution of this probe measured by ^1H NMR is of about 1 Hz, that is 5×10^{-9}. No external or internal lock is used, the field stability of the superconducting magnet being sufficient. The 90° pulse widths are 12 μs (^1H), 8 μs (^{13}C) and 17 μs (^{17}O). Finally, NMR signal to noise is improved by at least a factor of 10 compared with that obtained with the WP-60 high-pressure probes.[11]

Results and Data Treatment

A. Solvation of Ln^{3+} by DMF. In 1969 Soundarajan and Krishnamurthy[15] reported eight coordinate DMF complexes of lanthanide perchlorates (Ln = La, Ce, Pr, Nd, Sm) and we have subsequently confirmed that eight coordination in the solid state persists along the series to Lu.[6] In DMF, conductivity[16] and ^{35}Cl NMR[6] studies demonstrate that inner sphere complexation by ClO_4^- is absent. The only question that now arises is that of the coordination number of Ln^{3+} in DMF. Early visible spectrophotometric studies[17] of $Nd(ClO_4)_3$ in DMF and mixed H_2O–DMF solutions suggested that both NdO_8 and NdO_9 chromophores were present even at low water levels. Later infrared studies[16] of the C=O stretching vibration of DMF in $Ln(ClO_4)_3$/DMF/CH_3NO_2/H_2O solutions (Ln = Pr, Nd, Er) provided some support for the earlier spectrophotometric work and yielded maximum DMF coordination numbers of 9 for Pr, 8 for Nd, and 7 for Er. However, a direct determination of the coordination number (7.7 ± 0.2) in a $Tm(ClO_4)_3$/DMF/CD_2Cl_2 solution by NMR integration has been reported.[6] This possibility also exists for the Yb analogue as evidenced by the spectrum at 175 K in Figure 3. The coordination number in this case was found to be 7.8 ± 0.2 and indicates that the lowest coordination number in $Ln(ClO_4)_3$/DMF solutions is 8.

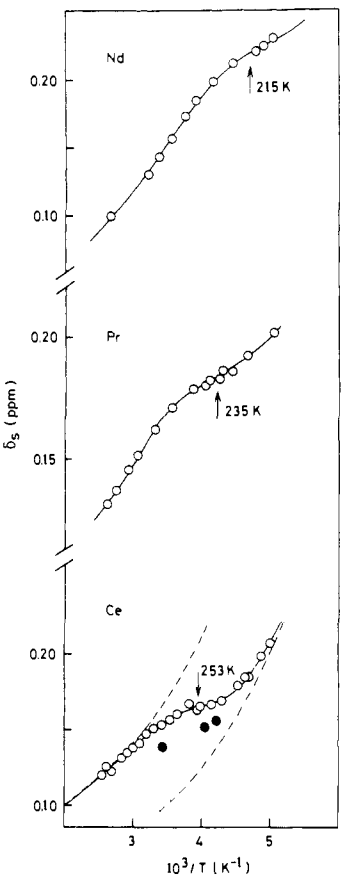

Figure 4. Plots of the paramagnetic induced NMR shift, δ_s (ppm), of the formyl proton in $[Ln(DMF)_8](ClO_4)_3$/DMF solutions (Ln = Ce–Nd) vs. inverse temperature. Open circles represent the ambient pressure shifts while the closed circles represent the cerium shifts at 200 MPa. The dashed curves indicate plausible shift variations with temperature of $[Ce(DMF)_8]^{3+}$ (upper curve) and $[Ce(DMF)_9]^{3+}$ species in solution. The approximate temperature corresponding to the inflection point of each experimental shift curve is also shown. The mole ratios of total DMF to Ln^{3+} are 145:1 (Ce), 161:1 (Pr) and 160:1 (Nd).

^1H NMR (formyl proton) shift evidence for an increase in coordination number above 8 for the lighter lanthanides, Ce–Nd in DMF is provided in Figure 4 and is explained as follows. The paramagnetic induced shift temperature dependence (vide infra) for a single solvated Ln^{3+} species can be described in terms of a monotonic cubic polynomial provided that solvent exchange is sufficiently fast, as is the case here. The fact that a point of inflection[18] is observed when Ln = Ce–Nd but not for Tb–Yb[6] implies that in the former systems two different paramagnetic environments contribute to the average ^1H shift of the solvent under conditions of rapid exchange. Since the contribution from

(14) Jonas, J. *Rev. Phys. Chem.* **1980**, *50*, 19.
(15) Krishnamurthy, S. S.; Soundararajan, S. *Can. J. Chem.* **1969**, *47*, 995.
(16) (a) Lugina, L. N.; Davidenko, N. K.; Zabotina, L. N.; Yatsimirskii, K. B. *Russ. J. Inorg. Chem.* **1974**, *19*, 1456. (b) Bünzli, J.-C. G.; Yersin, J.-R. *Helv. Chim. Acta* **1982**, *65*, 2498.
(17) Lugina, L. N.; Davidenko, N. K.; Yatsimirskii, K. B. *Russ. J. Inorg. Chem.* **1973**, *18*, 1453.
(18) The paramagnetic induced shift temperature dependence, when considered to be described by the weighted average of two monotonic cubic polynomials, should show a point of inflection when the contributions from the polynomials are approximately equal.

Table I. Calculated δ_S (ppm) Values (Extrapolated to $P_m = 1$) for $Ln(ClO_4)_3/S$ Solutions[a,b] (S = DMF, H_2O)

		^{17}O			^{13}C[c]	^{1}H[d]		
	$g_L - 1$	$Ln(DMF)_8^{3+}$[e]	$Ln(H_2O)_8^{3+}$	$Ln(H_2O)_9^{3+}$	$Ln(DMF)_8^{3+}$[f]	$Ln(DMF)_8^{3+}$[g]	$Ln(H_2O)_8^{3+}$	$Ln(H_2O)_9^{3+}$
Ce	$-1/7$	-9.4×10^1			−12	−2.76		
Pr	$-1/5$	-3.0×10^2	-3.8×10^2	-3.4×10^2	−17	−3.27	1.9	1.6
Nd	$-3/11$	-4.3×10^2	-4.9×10^2	-4.3×10^2	−27	−2.85	2.2	2.0
Tb	$1/2$	2.8×10^3	3.3×10^3	2.9×10^3	35	−63.6	−73	−65
Dy	$1/3$	2.5×10^3	2.6×10^3	2.3×10^3	29	−44.6	−48	−43
Ho	$1/4$	1.9×10^3	2.2×10^3	1.9×10^3	14	−27.9	−34	−30
Er	$1/5$	1.6×10^3	1.6×10^3	1.4×10^3	51	22.0	27	24
Tm	$1/6$	9.3×10^2	9.3×10^2	8.2×10^2	66	53.7	65	57
Yb	$1/7$	3.3×10^2	2.5×10^2	2.2×10^2	6.9	10.8	18	16

[a] Values for H_2O system refer to room temperature and are calculated from data in ref 5a. [b] Negative sign indicates downfield shift. [c] Carbonyl carbon. [d] Formyl proton for DMF. [e] At 299 K. [f] At 309 K. [g] Using internal benzene reference; at 295 K.

the environment generating the smaller downfield shift becomes more important at lower temperature (Figure 4) and because the solvent ^1H shift experienced in species such as $[Ln(DMF)_9]^{3+}$ would be predicted to be less pronounced than in $[Ln(DMF)_8]^{3+}$ (due to the increased metal–ligand distances), it appears that a species of coordination number greater than 8 is favored at lower temperature. Further, the variation of the temperature corresponding to the point of inflection with ionic radius of the lanthanide ion could be interpreted in terms of a destabilization of the higher coordination number species across the series, and this would be in line with expectations based on steric arguments. Finally, the effect of pressure on the cerium shifts is also consistent with an expected shift in equilibrium toward the species of higher coordination number. The probability of 10 coordination is not high in view of the spectroscopic work of Lugina et al.,[16] so that 9 coordination represents the highest coordination number attainable by Ln^{3+} in DMF.

In order to measure the equilibrium between $[Nd(DMF)_8]^{3+}$ and $[Nd(DMF)_9]^{3+}$ in DMF, and thus quantify the observations above, variable temperature and pressure visible spectrophotometric studies were carried out. The absorption band $^4I_{9/2} \rightarrow {}^2P_{1/2}$ in the electronic spectrum of Nd^{3+} is sensitive to environmental changes and, indeed, appears at 429.3 nm for $[Nd(DMF)_8]^{3+}$ (in agreement with Lugina et al.[17]) but at 428.2 nm for $[Nd(DMF)_9]^{3+}$. The temperature and pressure dependence of the two absorptions is such that the absorbance of $[Nd(DMF)_9]^{3+}$ becomes larger at lower temperature or higher pressure.[19] Figure 5 depicts the pressure dependence for a $[Nd(DMF)_8](ClO_4)_3$/DMF solution at 256 K. The thermodynamic parameters ΔH, ΔS, and ΔV[19] (-14.9 ± 1.3 kJ mol^{-1}, -69.1 ± 4.2 J K^{-1} mol^{-1}, and -9.8 ± 1.1 cm^3 mol^{-1}, respectively) associated with the reaction 1 were obtained by least-squares analysis[20] of the observed absorbance

$$[Nd(DMF)_8]^{3+} + DMF \underset{}{\overset{K}{\rightleftharpoons}} [Nd(DMF)_9]^{3+} \qquad (1)$$

changes with temperature and pressure, utilizing the relationships

$$\Delta H = T\Delta S - RT \ln K \qquad (2)$$

$$\Delta V = -RT(\partial \ln K/\partial P)_T \qquad (3)$$

Corrections for density changes and the temperature and pressure dependence of the extinction coefficients were made where necessary.[21] Figure 6 shows that results of the least-squares fit in

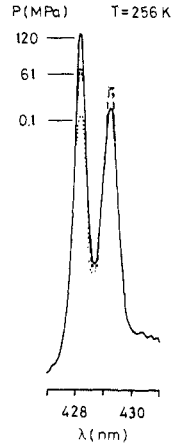

Figure 5. Visible spectra at 256 K of $[Nd(DMF)_8](ClO_4)_3$ in DMF ($[Nd^{3+}] \approx 0.1$ M) showing the effect of pressure on the equilibrium between $[Nd(DMF)_8]^{3+}$ (429.3 nm) and $[Nd(DMF)_9]^{3+}$ (428.2 nm). The solid curve, dashed curve, and dotted curve represent the spectra at 120 MPa, 61 MPa, and ambient pressure (0.1 MPa), respectively.

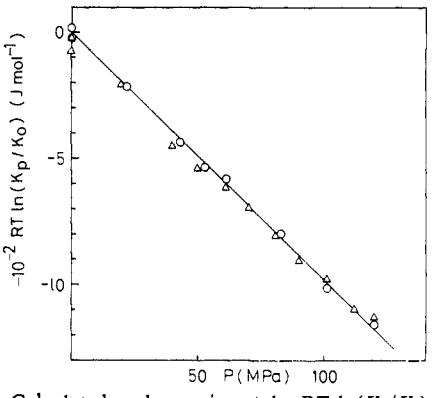

Figure 6. Calculated and experimental $-RT \ln(K_p/K_0)$ values as a function of pressure with the ratio of absorbances at 428.2 and 429.3 nm. Circles indicate data at 231 K, while triangles represent data at 256 K. ΔV was assumed to be temperature independent.

graphical form. The thermodynamic parameters may be compared with those for the addition of trimethylphosphate (TMP)[19] onto $[Nd(TMP)_6]^{3+}$: $\Delta H = -32.7 \pm 3.3$ kJ mol^{-1}, $\Delta S = -114 \pm 11$ J K^{-1} mol^{-1} and $\Delta V = -23.8 \pm 1.5$ cm^3 mol^{-1}. The difference in ΔH for the two reactions suggests a stronger metal–ligand bond for the TMP system. This may be rationalized in terms of the lower TMP coordination numbers (i.e., shorter metal–ligand bonds) but not in terms of the donicity difference between TMP and DMF (Gutmann Donor numbers for TMP and DMF are 23.0 and 26.6, respectively[22]) which would have suggested the contrary.

From the results of the present visible spectrophotometric and NMR shift studies it is relevant that equilibria between [Ln-

(19) Pisaniello, D. L.; Nichols, P. J.; Ducommun, Y.; Merbach, A. E. *Helv. Chim. Acta* **1982**, *65*, 1025.

(20) All temperature and pressure data were treated simultaneously. Actual absorbances from the variable temperature work formed one data set while absorbance ratios (428.2/429.3) from the variable pressure work constituted another set. Ratios are more sensitive when both species are present in rougly equal quantities.

(21) The small extinction coefficient temperature dependence for $[Nd(DMF)_8]^{3+}$ was established with solutions of $[Nd(DMF)_8](ClO_4)_3$ in either CH_3NO_2 or CH_2Cl_2. The spectra of these two solutions were identical and similar to the high-temperature spectra in neat DMF. The same temperature dependence was assumed to be valid for $[Nd(DMF)_9]^{3+}$. The extinction coefficient pressure dependence for $[Nd(DMF)_8]^{3+}$ was also small (ca. 5% increase/100 MPa) and assumed to be equal to that for $[Nd(DMF)_9]^{3+}$. Absorbance data are given in the supplementary material.

(22) Gutmann, V.; Schmid, R. *Coord. Chem. Rev.* **1974**, *12*, 263.

Table II. Derived NMR and Kinetic Parameters[a] for the Variable Temperature Study of DMF Exchange on $[Ln(DMF)_8]^{3+}$

	Tb[b]	Dy[c]	Ho[d]	Er[d]	Tm[b]	Yb[c]
ΔH^*, kJ mol^{-1}	14.09 (±0.4)	13.76 (±0.4)	15.31 (±0.8)	23.64 (±1.8)	33.18 (±0.5)	39.30 (±0.6)
ΔS^*, J K^{-1} mol^{-1}	−58.25 (±2.1)	−68.54 (±1.6)	−68.13 (±4.0)	−29.57 (±8.6)	9.85 (±2.4)	39.95 (±2.7)
k(298 K), s^{-1}	1.9 (±0.1) × 10^7	6.3 (±0.3) × 10^6	3.6 (±0.6) × 10^6	1.3 (±0.4) × 10^7	3.1 (±0.3) × 10^7	9.9 (±0.9) × 10^7
k(200 K), s^{-1}	7.9 (±0.2) × 10^5	2.8 (±0.1) × 10^5	1.16 (±0.02) × 10^5	8.0 (±0.3) × 10^4	2.94 (±0.09) × 10^4	2.78 (±0.09) × 10^4
A_m, s^{-1}	202 (±25)	435 (±33)	455 (±52)	265 (±32)	68 (±17)	10.6 (±2.4)
E_m, kJ mol^{-1}	2.5 (±0.3)	2.8 (±0.2)	1.5 (±0.3)	3.5 (±0.3)	7.0 (±0.7)	5.9 (±0.6)
B_1, rad s^{-1} K^e	1.1 (±0.1) × 10^7	2.7 (±0.3) × 10^6	3.6 (±0.3) × 10^6	3.7 (±0.5) × 10^6	1.1 (±0.2) × 10^7	9.0 (±2.6) × 10^5
B_2, rad s^{-1} K^2 [e]	−6.4 (±0.6) × 10^9	−8.5 (±1.7) × 10^8	−2.0 (±0.1) × 10^9	−2.9 (±0.3) × 10^9	−9.0 (±0.9) × 10^9	−8.2 (±1.4) × 10^8
B_3, rad s^{-1} K^3 [e]	1.45 (±0.07) × 10^{12}	3.8 (±0.2) × 10^{11}	5.1 (±0.2) × 10^{11}	7.1 (±0.3) × 10^{11}	2.1 (±0.1) × 10^{12}	2.5 (±0.2) × 10^{11}
C_1	0.16[f]	0.16[f]	0.16[f]	0.16[f]	0.171 (±0.004)	0.158 (±0.008)

[a] The errors represent one standard deviation. [b] Combined 200/60 MHz fit. [c] Combined 360/60 MHz fit. [d] 60 MHz fit. [e] At 60 MHz. [f] Fixed at this value.

$(DMF)_8]^{3+}$ and $[Ln(DMF)_9]^{3+}$ species do exist for the light lanthanides. It is also evident that at room temperature the major species is $[Ln(DMF)_8]^{3+}$ when Ln = Ce–Nd and this becomes the only stable species when Ln = Tb–Lu. As alluded to in the Introduction, the question of whether there is a change in coordination number for lanthanide aquoions has remained open for many years. Spedding and co-workers[4] have concluded that a changeover occurs in the region of Sm^{3+} at room temperature. Our results would support their conclusions since it is to be expected on steric grounds that the formation of a $[LnS_9]^{3+}$ species would be more favorable when S = H_2O than when S = DMF.

B. Characteristic ^1H, ^{13}C and ^{17}O Shifts. The characteristic lanthanide induced shifts for ^1H, ^{13}C and ^{17}O nuclei in $Ln(ClO_4)_3$/DMF solutions have been measured and are presented in Table I. Here δ_S is the chemical shift in ppm between solvent nuclei in the paramagnetic environment and in pure DMF. Corresponding ^{17}O and ^1H shifts for aqueous solutions when the coordination number is either 8 or 9 are also presented for comparison. In general, the isotropic shift of nuclei in lanthanide complexes is given by the sum of the Fermi contact and pseudo-contact interactions. According to Reuben and Fiat,[5a] the contact contribution is given by

$$\Delta\nu/\nu_0 = \frac{2\pi\beta J(J+1)g_L(g_L-1)}{3kT\gamma N}\frac{A}{h} \quad (4)$$

where A/h is the scalar coupling constant in Hz and g_L is the Landé g factor, all other symbols having their usual meaning. For lanthanide complexes having axial symmetry the pseudo-contact shifts have been predicted[23] to be proportional to

$$\frac{D_z(3\cos^2\theta - 1)}{r^3T^2} \quad (5)$$

where D_z is the axial component of the zero field splitting tensor and θ is the angle between the vector of length r joining the nucleus to the metal ion and the principal axis of symmetry. From Table I the sign and magnitude of g_L have a good correlation with those of the observed ^{17}O shift and this is consistent with a dominant contact shift contribution. Reuben and Fiat[5a] have made a similar conclusion for the aqueous systems. The signs of the ^{13}C shifts suggest a significant contact contribution but the shift magnitude correlation with $|g_L - 1|$ is poor, indicating a substantial pseudo-contact (dipolar) contribution to the carbonyl carbon shift. In the case of the formyl ^1H shift it is clear that the dipolar interaction is dominant (cf. Tb). A similar conclusion has been reached[5a] for the water proton in the aqueous systems. Finally, the close similarity in the ^{17}O shift values for H_2O and DMF systems probably reflects a similar scalar coupling interaction between the paramagnetic center and the ^{17}O nucleus.

C. Variable Temperature Kinetics. The Swift and Connick approach[24] was used to determine kinetic parameters for those lanthanide systems where exchange broadening was evident (Tb–Yb). The relevant equations have been previously presented[6] but are repeated here for convenience. The transverse NMR relaxation time, T_2, and the chemical shift (relative to that of pure DMF), $\Delta\omega_s$ (rad s^{-1}) for the free or coalesced DMF signal (formyl proton in this work) are dependent on various parameters as follows.[25]

$$\frac{1}{T_{2r}} = \frac{1}{P_m}\left(\frac{1}{T_2} - \frac{1}{T^0_{2A}}\right) = \frac{1}{\tau_m}\left[\frac{T_{2m}^{-2} + (T_{2m}\tau_m)^{-1} + \Delta\omega_m^2}{(T_{2m}^{-1} + \tau_m^{-1})^2 + \Delta\omega_m^2}\right] + \frac{1}{T_{2os}} \quad (6)$$

$$\Delta\omega_r = \frac{\Delta\omega_s}{P_m} = \frac{\Delta\omega_m}{(\tau_m/T_{2m} + 1)^2 + \tau_m^2\,\Delta\omega_m^2} + \Delta\omega_{os} \quad (7)$$

where T^0_{2A} is the relaxation time of pure DMF, T_{2m} is the relaxation time of coordinated DMF in the absence of exchange, P_m is the mole fraction of coordinated DMF, τ_m is the residence time of a coordinated DMF ligand, $\Delta\omega_m$ is the chemical shift between free (bulk) and coordinated DMF in the absence of exchange, and $\Delta\omega_{os}$ is the chemical shift between pure DMF and bulk DMF. The T_{2os} term in eq 6 was neglected in the data treatment since no significant outer-sphere relaxation for Tb–Yb systems was apparent.[6] The $\Delta\omega_{os}$ term is, however, significant and reflects in part the characteristics of the internal benzene reference[6] used in this work. It was assumed to be related to $\Delta\omega_m$ by

$$\Delta\omega_{os} = C_1\Delta\omega_m \quad (8)$$

The temperature dependence of $\Delta\omega_m$, itself, may be described empirically as a power series of $1/T$,[25-27] but only the first three terms will be considered, i.e.

$$\Delta\omega_m = B_1/T + B_2/T^2 + B_3/T^3 \quad (9)$$

The inner-sphere relaxation time is assumed to have a simple temperature dependence given by

$$1/T_{2m} = A_m\exp(E_m/RT) \quad (10)$$

while τ_m may be related to the pseudo-first-order exchange rate constant, k, and temperature by the Eyring equation

$$k = 1/\tau_m = k_BT/h\exp(\Delta S^*/R - \Delta H^*/RT) \quad (11)$$

Figure 7 shows the temperature dependence of ln $(1/T_{2r})$ and $\Delta\omega_r$ for the lanthanide systems studied. The NMR and kinetic parameters obtained by a nonlinear least-squares analysis of the data, using eq 6–11, are listed in Table II. The outer-sphere parameter, C_1, was optimized in the cases of the relatively slowly exchanging Tm and Yb systems but fixed at 0.16 for Tb–Er because it is not expected to change markedly for these complex ions which are of similar size. The statistical correlation between ΔH^* and ΔS^* was found to be almost unity, as expected,[25] but the correlation between either of these two parameters with A_m, E_m, B_1, B_2, B_3 or C_1 was generally less than 0.3. Where data at two different

(23) Bleaney, B. *J. Magn. Reson.* **1972**, *8*, 91.
(24) Swift, T. J.; Connick, R. E. *J. Chem. Phys.* **1962**, *37*, 307.
(25) Newman, K. E.; Meyer, F. K.; Merbach, A. E. *J. Am. Chem. Soc.* **1979**, *101*, 1470.
(26) McGarvey, B. R. *J. Magn. Reson.* **1979**, *33*, 445.
(27) Lee, L.; Sykes, B. D. *J. Magn. Reson.* **1980**, *41*, 512.

Table III. Formyl Proton Relaxation Rates, $1/T_{2r}$, Chemical Shifts, $\Delta\omega_r$, and Rate Constants k for DMF Exchange on $[Ln(DMF)_8]^{3+}$ in the Diluent CD_3NO_2 at 200 MHz

mol % DMF[a]	$[DMF]_{free}$[b]	$1/T_{2r}$, s^{-1}	$\Delta\omega_r$, rad s^{-1}	k, s^{-1}	$1/T_{2r}$, s^{-1}	$\Delta\omega_r$, rad s^{-1}	k, s^{-1}
Ln = Terbium (P_m = 0.0500):			T = 231.1 K[c]			T = 239.2 K[d]	
2	0.30	50 700	1.26×10^5	0.382×10^6	33 800	1.23×10^5	0.506×10^6
4	1.17	18 200	1.52×10^5	1.24×10^6	12 900	1.39×10^5	1.46×10^6
14	2.04	13 000	1.57×10^5	1.78×10^6	9 500	1.45×10^5	2.01×10^6
20	2.89	11 400	1.64×10^5	2.08×10^6	7 900	1.50×10^5	2.47×10^6
100[g]	13.68	8100	1.72×10^5	2.96×10^6	5 400	1.55×10^5	3.78×10^6
Ln = Thulium (P_m = 0.0250):			T = 242.1 K[e]			T = 247.6 K[f]	
2	0.30	24 000	0.99×10^5	0.78×10^6	18 300	0.92×10^5	0.87×10^6
4	1.17	25 500	1.11×10^5	0.73×10^6	16 500	1.02×10^5	0.98×10^6
14	2.04	23 500	1.15×10^5	0.80×10^6	15 800	1.06×10^5	1.03×10^6
20	2.89	22 600	1.20×10^5	0.84×10^6	15 800	1.10×10^5	1.06×10^6
100[g]	13.68	17 400	1.53×10^5	1.14×10^6	10 500	1.39×10^5	1.69×10^6

[a] $[DMF]_t/[DMF]_t + [CD_3NO_2]$ in %. [b] In mol/kg of solvent (total DMF + CD_3NO_2), excluding the reference (1% benzene). [c] $1/T_{2m}$ = 737.8 s^{-1} and $\Delta\omega_m = 1.485 \times 10^5$ rad s^{-1}. [d] $1/T_{2m}$ = 710.2 s^{-1} and $\Delta\omega_m = 1.336 \times 10^5$ rad s^{-1}. [e] $1/T_{2m}$ = 2203 s^{-1} and $\Delta\omega_m = 1.33 \times 10^5$ rad s^{-1}. [f] $1/T_{2m}$ = 2039 s^{-1} and $\Delta\omega_m = 1.20 \times 10^5$ rad s^{-1}. [g] The data in neat solvents are calculated from the parameters in Table II.

Table IV. Derived NMR and Kinetic Parameters[a] for the Variable Pressure Study of DMF Exchange on $[Ln(DMF)_8]^{3+}$

	Tb[b]	Dy[c]	Ho[d]	Er[e]	Tm[f]	Yb[g]
ΔV^*, cm^3 mol^{-1}	5.2 ± 0.2	6.1 ± 0.2	5.2 ± 0.5	5.4 ± 0.3	7.4 ± 0.3	11.8 ± 0.4
$10^2\Delta\beta^*$, cm^3 mol^{-1} MPa^{-1}	−0.9 ± 0.7	−0.7 ± 0.5	−0.3 ± 1.0	0.2 ± 0.9	0.03 ± 0.9	2.0 ± 0.9
10^4P_1, MPa^{-1}	4.30 ± 0.07	4.2 ± 0.1	6.0 ± 0.4	6.3 ± 0.3	5.7 ± 0.2	5.82 ± 0.07
10^4P_2, MPa^{-1}	13 ± 7	13 ± 2	29 ± 5	7 ± 3	7 ± 2	9 ± 5

[a] The errors represent one standard deviation. [b] 235 K. [c] 236 and 240 K. [d] 234 and 239 K. [e] 236 and 241 K. [f] 255 K. [g] 235 and 240 K.

field strengths were combined (Tb, Dy, Tm, Yb) in a single least-squares analysis, it was assumed that T_{2m} was independent of field strength (from Figure 7 there is no visible field dependence of T_{2m} for the high temperature ln $(1/T_{2r})$ data). While some field effect cannot be ruled out entirely for these systems, it is clear that the 60-MHz data considered alone would be well-fitted by the relevant NMR and kinetic parameters quoted in Table II. The parameter, E_m, can be related to the activation energy for electron spin relaxation if simple dipolar relaxation is involved (i.e., $T_1 = T_2$)[28] and it is found that the values of E_m in Table II are similar to those reported recently[29] for lanthanide aquo ions.

In Table III are reported the experimental formyl proton $1/T_{2r}$ and $\Delta\omega_r$ values for DMF exchange on $[Ln(DMF)_8]^{3+}$ (Ln = Tb and Tm) in the inert diluent nitromethane. The rate constants $k = 1/\tau_m$ were derived using eq 6 and taking for $1/T_{2m}$ and $\Delta\omega_m$ the values calculated from eq 9 and 10 with the relevant parameters in Table II; the T_{2os} term is neglected as above. $\Delta\omega_r$ values could not be used to calculate the k values, mainly because $1/\tau_m^2 \gg 1/T_{2m}^2$, $\Delta\omega_m^2$ and also because $\Delta\omega_{os}$ varies with the concentration of free DMF in a nonquantifiable manner. As expected, the dilution produces a decrease in $\Delta\omega_r$, essentially due to the large increase in the $\Delta\omega_{os}$ term.

D. Variable Pressure Kinetics. It was found that the lowest feasible temperature for variable pressure work (to 200 MPa) with the DMF solutions (0.1 m Ln^{3+}) was about 230 K. At 60 MHz the chemical exchange broadening did not constitute the major contribution to the total formyl ^1H line width in this temperature region and hence accurate volume information could not be obtained by using the 60-MHz instrument alone. This necessitated working at higher field (200 MHz) for which the $\Delta\omega_m\tau_m^2$ term becomes a much more important[25] contribution to $1/T_{2r}$. It was decided to work with both instruments and maintain equal temperatures for the two experiments: the sample temperatures at any particular pressure would be identical if the formyl proton chemical shifts (ppm) from the internal benzene reference were the same on both instruments and sufficiently rapid DMF exchange was occurring at that temperature (i.e., $\Delta\omega_r = \Delta\omega_m + \Delta\omega_{os}$). The former condition could be met easily by minor temperature adjustment before the start of the variable pressure experiment at the second field strength. The latter condition could also be easily met by the correct choice of temperature for the experiments (Figure 7).

Variable pressure data were analyzed by least squares in terms of eq 6–8 and also the following equations

$$\Delta V^* = \Delta V_0^* - \Delta\beta^* P \quad (12)$$

$$\ln k_P = \ln k_0 - \Delta V_0^* P/RT + \Delta\beta^* P^2/2RT \quad (13)$$

$$\Delta\omega_{mp} = \Delta\omega_{m0}(1 + P_1 P) \quad (14)$$

$$T_{2mp}^{-1} = T_{2m_0}^{-1}(1 + P_2 P) \quad (15)$$

where ΔV^* is the pressure independent volume of activation, ΔV_0^* is the zero pressure volume of activation, $\Delta\beta^*$ is the compressibility coefficient of activation, k_0, $\Delta\omega_{m_0}$, $T_{2m_0}^{-1}$ refer to zero pressure and k_P, $\Delta\omega_{mP}$ and T_{2mP}^{-1} refer to the actual pressure.[30] The parameters P_1 and P_2 are used to take into account small changes in $\Delta\omega_m$ and T_{2m}^{-1} with pressure. Figure 8 shows, in graphical form, the experimental (200-MHz data) and calculated $-RT\ln(k_P/k_0)$ values versus pressure while Table IV lists the relevant parameters. Data from two similar, but not identical temperatures were used to define common activation volumes in the Dy–Er and Yb cases. Some T_{2m}^{-1} increase with pressure occurs[31] and, interestingly, an increase in $\Delta\omega_m$ as well. Few reports of the pressure dependence of NMR shifts have been made[32] and these have been mainly for diamagnetic systems. The P_1 values do not vary greatly across the lanthanides (some systematic error could be present) and could reflect slight ligand distortion in the first coordination sphere with pressure. Finally, $\Delta\beta^*$ is not statistically significant and hence

(28) Burns, P. D.; la Mar, G. N. *J. Magn. Reson.* **1982**, *46*, 61.
(29) Alsaadi, B. M.; Rossotti, F. J. C.; Williams, R. J. P. *J. Chem. Soc. Dalton Trans.* **1980**, 2147.

(30) The parameters optimized were ΔV^* (or ΔV_0^* and $\Delta\beta^*$), P_1, P_2, $\Delta\omega_{m_0}$, $T_{2m_0}^{-1}$, and k_0. Details are given in the supplementary material.
(31) T_{2m} was assumed to be independent of field strength in the determination of ΔV^*. However, as mentioned before, some dependence cannot be entirely ruled out and the effect could be significant in the evaluation of ΔV^* where the most important data are obtained at 200 MHz. The ambient pressure line widths are consistent with no field dependence, but, in order to allow for T_{2m} field dependence at higher pressures, P_2 for 60-MHz data was multiplied by a fixed constant and this P_2 value applied for the 200-MHz data, the effect on ΔV^* being noted. For a factor of 3, the ΔV^* was reduced by 0.2 cm^3 mol^{-1}, which is within the estimated experimental error of 1–2 cm^3 mol^{-1} (including nonrandom errors) associated with ΔV^*.
(32) Yamada, H.; Itani, C.; Otsuka, K. *J. Am. Chem. Soc.* **1977**, *99*, 3572.

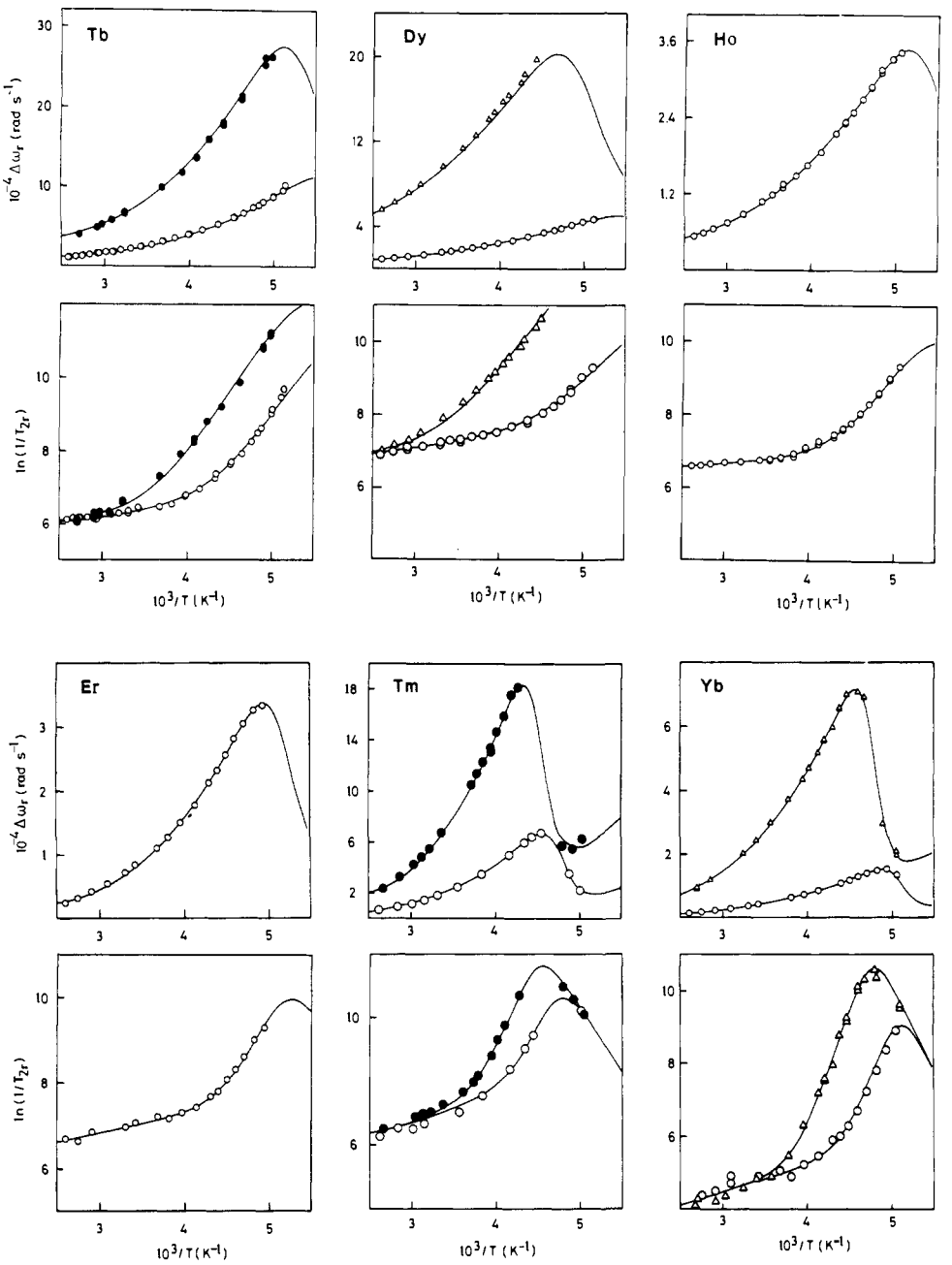

Figure 7. Variable temperature ^1H NMR data for $[Ln(DMF)_8](ClO_4)_3$ in DMF (Ln = Tb–Yb): shifts and line widths vs. inverse temperature: (○) 60 MHz $\Delta\omega_r$ and ln $(1/T_{2r})$; (●) 200 MHz $\Delta\omega_r$ and ln $(1/T_{2r})$; (△) 360 MHz $\Delta\omega_r$ and $\ln 1/T_{2r}$. Full details are given in the supplementary material.

ΔV^*, the pressure independent volumes of activation, are quoted in Table IV.

Discussion

The overall labilities of $[Ln(DMF)_8]^{3+}$ ions are high (Table II) but generally less than the labilities of the aquoions for which rate constants of $>10^8$ s^{-1} have been measured[33] or estimated[3,34] at room temperature. Such behavior is in accord with a general trend, namely that for the vast majority of metal ions, the rate of nonaqueous solvent exchange and, in particular DMF exchange, is lower than that of water exchange. If a single exchange mechanism were operative for all $[Ln(DMF)_8]^{3+}$ species similar labilities would be expected since the ionic radii of Ln^{3+} are only marginally different. It has been found that the DMF exchange rates measured at low temperatures (ca. 200 K) are substantially different among the heavy lanthanides and this coupled the trends in ΔH^*, ΔS^*, and ΔV^* with the ionic radius of Ln^{3+} (Figure 9) strongly suggests that the mechanism of exchange varies along the series. Further evidence for a variation in mechanism comes from the observed coexistence of $[Ln(DMF)_8]^{3+}$ and $[Ln(DMF)_9]^{3+}$ in DMF solutions of the light lanthanides (Ce–Nd). Increasing steric interaction between coordinated ligands is probably responsible for the shift in equilibrium toward $[Ln(DMF)_8]^{3+}$ across the series, and hence it may also determine to a large degree the mechanism of exchange by favoring one intermediate or transition state over another in a progressive manner. The sign and magnitude of activation parameters for the exchange of DMF on individual $[Ln(DMF)_8]^{3+}$ ions should give an indication of the type of mechanism operating,[35] but the apparent conflict in ΔS^* and ΔV^* for Tb–Er precludes any obvious assessment for these ions.

The kinetic results obtained in nitromethane diluent (Figure 10) are therefore now considered, and are mechanistically very informative. For $[Tm(DMF)_8]^{3+}$ the exchange rate constants are practically independent of the free DMF concentration. Their

(33) Southwood-Jones, R. V.; Earl, W. L.; Newman, K. E.; Merbach, A. E. *J. Chem. Phys.* **1980**, *73*, 5909.
(34) Fay, D. P.; Litchinsky, D.; Purdie, N. *J. Phys. Chem.* **1969**, *73*, 544.
(35) Merbach, A. E. *Pure Appl. Chem.* **1982**, *54*, 1479.

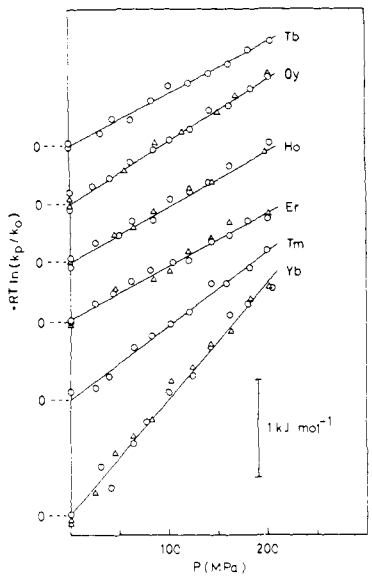

Figure 8. Calculated and experimental $-RT \ln (k_p/k_o)$ values as a function of pressure by use of eq 6–8 and 12–15. ΔV^* is assumed to be pressure independent. The triangles represent data associated with the higher of the two temperatures studied for the Dy, Ho, Er, and Yb systems (Table IV). The origin for each system is indicated at the left of the figure.

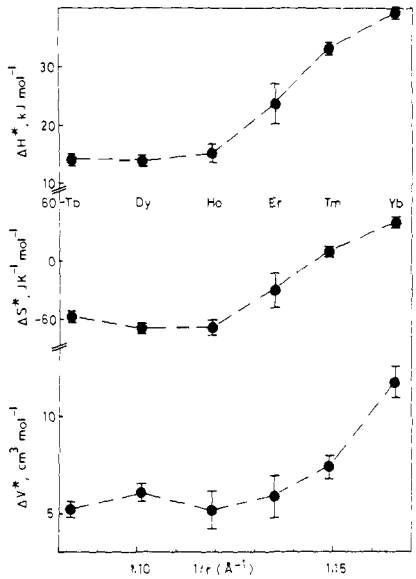

Figure 9. Activation parameters for DMF exchange on $Ln(DMF)_8^{3+}$ in neat solvent.

slight increase from dilute solution in nitromethane to neat DMF can be ascribed to changes in the bulk properties of the solvent. The observed first order rate law

$$-d[Tm(DMF)_8^{3+}]/([Tm(DMF)_8^{3+}]dt) = 8k = k_D \quad (16)$$

is consistent with the operation of a dissociative mechanism D whereby an intermediate of reduced coordination number 7 is formed according to the reaction scheme

$$[Tm(DMF)_8]^{3+} \xrightarrow{k_D} \{Tm(DMF)_7\}^{3+} + DMF$$

$$\{Tm(DMF)_7\}^{3+} + *DMF \xrightarrow{fast} [Tm(DMF)_7(*DMF)]^{3+} \quad (17)$$

For both Tm and Yb the ΔS^* are consistent with a dissociative activation mode. On the basis of the close similarity of ΔV^* for Yb and the ΔV for the dissociation reaction of $[Nd(DMF)_9]^{3+}$ ($+9.8 \pm 1.1$ cm^3 mol^{-1}) it is evident that the mechanism for DMF exchange on $[Tm(DMF)_8]^{3+}$ and $[Yb(DMF)_8]^{3+}$ is essentially the limiting dissociative D mechanism. In contrast, for $[Tb(DMF)_8]^{3+}$ the observed exchange rate constants in nitromethane

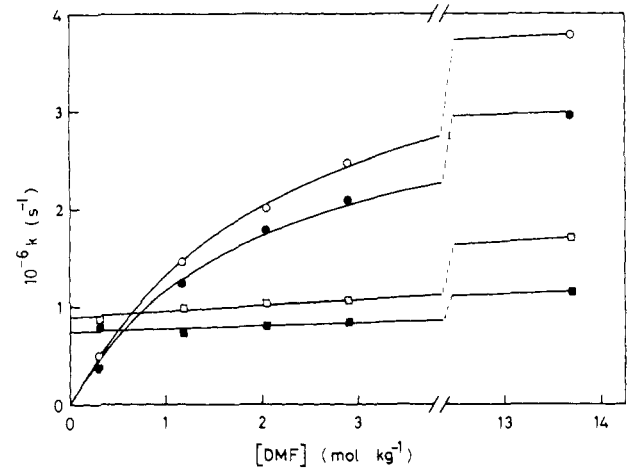

Figure 10. Rate constants k for DMF exchange on $[Ln(DMF)_8]^{3+}$ in the diluent CD_3NO_2: (a) Ln = Terbium (p_m = 0.0500) at 231.1 K (●) and 239.2 K (○); the solid lines are fit of the data according to eq 19; (b) Ln = Thulium (p_m = 0.0250) at 242.1 K (■) and 247.6 K (□); the dashed lines are linear fit of the data.

first increase almost proportionally with the concentration of free DMF and finally level at the value observed in neat DMF. This behavior can be interpreted in terms of an interchange mechanism I according to reaction scheme 18. The observed exchange rate

$$[Tb(DMF)_8]^{3+} + DMF \overset{k_{os}}{\rightleftharpoons} [Tb(DMF)_8{}^{3+} \ldots *DMF] \quad (18)$$

$$[Tb(DMF)_8{}^{3+} \ldots *DMF] \xrightarrow{k_1} [Tb(DMF)_7(*DMF)^{3+} \ldots (DMF)]$$

constant k is related to K_{os}, the equilibrium constant for the formation of the outer-sphere complex, and to k_1, the rate constant for the interchange step, by eq 19. The solid lines in Figure 10

$$-d[Tb(DMF)_8{}^{3+}]/([Tb(DMF)_8{}^{3+}]dt) = 8k = k_1K_{os}[DMF]/(1 + K_{os}[DMF]) \quad (19)$$

are the results of least square fit and corresponds to K_{os} values of 0.51 ± 0.05 (231.1 K) and 0.42 ± 0.01 (239.2 K) mol^{-1} kg. These values agree well with estimates of K_{os} from the Fuoss–Eigen equation[36] which are slightly less than unity for neutral ligands. The apparent conflict in ΔS^* and ΔV^* for Tb, Dy, and Ho in neat solvent is now easier to rationalize. The negative ΔS^* are consistent with a decrease in degrees of freedom accompanying the formation of a nine coordinate transition state. The interpretation of ΔV^* is simplified due to the absence of electrostrictive changes. The positive values may be thought to arise from the sum of two opposite effects: a negative contribution due to the penetration of the ninth ligand into the first coordination sphere and a dominant positive contribution arising from bond lengthening for the leaving ligand and for the nonexchanging ligands to reach the transition state. Increase in chemical shift when comparing the eight coordination with the ninth coordinate solvates (Figure 4) supports the contribution from metal–ligand bond lengthening. According to their positive ΔV^*, a dissociative activation mode could operationally[37] be assigned to the interchange, I, on Tb, Dy, and Ho. It is also expected that the activation mode becomes more associative when moving toward the lighter lanthanides, for which finally the nine coordinate transition state becomes a stable ground state. For Tb the possibility of exchange occurring by two competing pathways (simultaneous D and A mechanisms) could be eliminated from the rate law and also because ΔV^* does not exhibit the expected variation[38] with T. In conclusion, DMF exchange occurs through an interchange I mechanism for Tb to Er, through

(36) Fuoss, R. J. *J. Am. Chem. Soc.* **1958**, *80*, 5059.
(37) Swaddle, T. W. *Rev. Phys. Chem.* **1980**, *50*, 230.
(38) ΔV^* would be expected to become more positive with increase in temperature. For Tb^{3+}, $\Delta V^* = 6.2 \pm 0.5$ at 221 K and 3.3 ± 0.4 at 260 K.

a *D* mechanism for Tm and Yb, and a mechanistic crossover occurs at Er.

Acknowledgment. The authors express their thanks to R. Ith, P. Pollien, and R. Tschanz for their machine work in the construction of the high-pressure probe-heads and for their valuable suggestions regarding design. This work was supported by the Swiss National Science Foundation under grand 2.256-0-81.

Registry No. DMF, 68-12-2; $Ce(DMF)_8^{3+}$, 45316-14-1; $Pr(DMF)_8^{3+}$, 45316-20-9; $Nd(DMF)_8^{3+}$, 45316-19-6; $Tb(DMF)_8^{3+}$, 51232-27-0; $Dy(DMF)_8^{3+}$, 51223-48-4; $Ho(DMF)_8^{3+}$, 51232-29-2; $Er(DMF)_8^{3+}$, 51232-31-6; $Tm(DMF)_8^{3+}$, 51232-33-8; $Yb(DMF)_8^{3+}$, 51232-35-0; ^{17}O, 13968-48-4.

Supplementary Material Available: Experimental data for the temperature and pressure dependence of pure DMF (Table SI) and $Ln(ClO_4)_3$ solutions (Tables SII to SVII), formyl proton relaxation rates, and chemical shifts; detailed results and correlation coefficient matrix of the least-squares analysis of NMR data (Table SVIII); experimental data for the variable temperature and pressure study of Nd^{3+} by spectrophotometry (Table SIX) (31 pages). Ordering information is given on any current masthead page.

Surface Spectroscopic Studies of Polymer Surfaces and Interfaces: Poly(tetramethyl-*p*-silphenylenesiloxane)

Joseph A. Gardella, Jr.,*† J. S. Chen,‡ J. H. Magill,‡ and David M. Hercules*

Contribution from the Departments of Chemistry and Metallurgical and Materials Engineering, University of Pittsburgh, Pittsburgh, Pennsylvania 15260. *Received August 5, 1982*

Abstract: Surface spectroscopic (ESCA, FTIR) studies of changes in the morphology of fractionated poly(TMpS) solution-grown crystal mats (I), melt-cast mats (II), melt-quenched mats (III), and solution-cast films (IV) have been correlated with thermal (differential scanning calorimetry), crystallographic (small angle X-ray scattering), and gas phase (HF) reaction studies. These results provide a complete picture of the surface structure of this well-ordered macromolecular material, demonstrating for the first time the use of ESCA to analyze the morphology of an ordered homopolymer. ESCA analyses of various degrees of crystallinity of poly(TMpS) (I > II > III > IV) were correlated with FTIR results yielding the conclusion that the surface (amorphous) region of each material consists of surface-segregated Si–C_6H_4–Si–O linkages, most likely in the form of folds or loops of the long chains back into the rod-like crystalline core of the materials. Chemical etching studies were accomplished with gaseous HF (diluted with He 10:30 v/v) which selectively reacts with and removes the less-ordered surface amorphous regions, thereby increasing the overall crystallinity. This process was followed both spectroscopically and with DSC and SAXS analysis, providing results which demonstrate the efficacy of these methods and confirm the surface chemistry and morphology of the polymer system.

Introduction

Elucidation of structure–property relationships in polymeric materials is a goal of much research which is intent on development of property specificity in polymers. Chemical structure at the monomer level and in the polymer chain itself have been shown to be important determinants of various physical properties. The study of ordered or crystalline polymers constitutes one important aspect of these studies.

Since Palmer and Cobbald[1] first discovered that warm, concentrated nitric acid preferentially attacks the less-ordered regions in polyethylene (PE), chemical degradation studies have been conducted to probe the morphology of crystalline polymers. For instance, investigations by Peterlin and Meinel[2] and Priest and Keller[3] on polyethylene, isotactic polypropylene by Hock,[4] and cellulose by Manley[5] have shown that structure–property relationships may be obtained by using chemical degradation as a structural probe. More recent work on crystalline polyethylene[6,7] has provided information on the morphology of polyethylene single crystals.

Spectroscopic analysis is common for deducing polymer structure.[8] Recently, Fourier transform infrared spectroscopy (FTIR) has been used, especially for studying polymer morphology of crystalline polyethylene.[9-11] Advantages such as high spectral resolution, reproducibility in band position and intensity, signal to noise enhancement, and data processing capabilities have made FTIR one of the most suitable techniques for studying the relatively small spectral changes associated with polymer morphology and corresponding crystallinity features. X-ray photoelectron spectroscopy (XPS or ESCA) has also been used extensively in the analysis of the chemical structure of polymers.[12,13] ESCA is sensitive to surface structure (10–50 Å) and compares favorably with other surface spectroscopic measurements[14] in its ability to distinguish between structural differences in homopolymers. However, it frequently lacks definitive interpretation when utilized alone. For this reason, it is best to use ESCA with other spec-

* Department of Chemistry.
† Department of Chemistry, State University of New York at Buffalo, Buffalo, NY 14214.
‡ Department of Metallurgical and Materials Engineering.

(1) Palmer, R. P.; Cobbald, A. *Macromol. Chem.* **1964**, *74*, 174.
(2) Peterlin, A.; Meinel, G. *J. Polym. Sci., Part B* **1965**, *3*, 9.
(3) Priest, D. J. *J. Polym. Sci. Part A2* **1971**, *9*, 1777; Keller, A.; Priest, D. J. *J. Macromol. Sci. (B)* **1968**, *2*, 479.
(4) Hock, W. W. *J. Polym. Sci. Phys.* **1965**, *3*, 573; *J. Polym. Sci., Part A2*, **1966**, *4*, 227.
(5) Manley, R. St. J. *J. Polym. Sci. Polym. Phys. Ed.* **1974**, *12*, 1347.
(6) Keller, A.; Martuscelli, E.; Priest, d. J.; Udagawa, Y. *J. Polym. Sci., Part A* **1971**, *9*, 1807.
(7) Patel, G. N.; Keller, A. *J. Polym. Sci. Polym. Phys. Ed.* **1975**, *13*, 22.
(8) Hummel, D. O. "Infrared Analysis of Polymers, Resins and Additives, An Atlas"; Wiley-Interscience: New York, 1971.
(9) Painter, P. C.; Havens, J.; Hart, W. W.; Koenig, J. L. *J. Polym. Sci., Polym. Phys. Ed.* **1977**, *15*, 1223.
(10) Bank, M. I.; Krimm, S. *J. Polym. Sci. Part A2* **1969**, *7*, 1785.
(11) Ching, J. H. C.; Krimm, S. *J. Appl. Phys.* **1975**, *46*, 4181.
(12) Clark, D. T. "Handbook of X-ray and Ultraviolet Photoelectron Spectroscopy"; D. Briggs, Ed.; Heyden: London, 1972; pp 211-247.
(13) Dwight, D. W. "Photon, Electron and Ion Probes of Polymer Structures and Properties"; Dwight, D. W.; Fabish, T. J.; Thomas, H. R., Ed.; American Chemical Society: Washington, DC, 1981.
(14) Gardella, J. A., Jr.; Hercules, D. M. *Anal. Chem.* **1981**, *53*, 1879.

0002-7863/83/1505-4536$01.50/0